Journal of Alloys and Compounds 688 (2016) 62–68

Contents lists available at ScienceDirect

Journal of Alloys and Compounds

journal homepage: http://www.elsevier.com/locate/jalcom

Grain size effect on stress hysteresis of nanocrystalline NiTi alloys

X.B. Shi [a, b], F.M. Guo [b], J.S. Zhang [b, c], H.L. Ding [a], L.S. Cui [b, *]

[a] School of Materials Science and Engineering, Anhui University of Technology, Maanshan 243002, China
[b] State Key Laboratory of Heavy Oil Processing, China University of Petroleum, Beijing, Changping 102249, China
[c] Institute for Advanced Materials, Jiangsu University, Zhenjiang 212013, China

ARTICLE INFO

Article history:
Received 16 March 2016
Received in revised form
15 July 2016
Accepted 16 July 2016
Available online 18 July 2016

Keywords:
Grain size effect
Hysteresis
Nanocrystalline NiTi alloy
Microstructures
Stress-induced transformation

ABSTRACT

In this paper, the grain size effect on the stress hysteresis of a nanocrystalline NiTi alloy during superelastic cycling was investigated by testing two types of samples with 39% and 75% cold-drawn area reduction. The TEM microstructure and DSC analysis reveal that the sample with 75% area reduction experiences a crystallization process upon heating and contains few dislocations after annealing. The activation energy for grain boundary migration of the NiTi alloy was analysed and found to be 353.6 ± 15.3 kJ/mol. The hysteresis analysis shows that the stress hysteresis of the samples after annealing increases with decreasing grain size. We propose that the energy dissipation per volume of grain boundary is larger than that of the grain core in the nanocrystalline NiTi alloy, which contributes to this grain size effect. However, the sample with 39% area reduction does not experience the crystallization process upon heating, and many dislocations are encountered in the samples after annealing. The stress hysteresis of the samples with 39% area reduction after annealing decreases with increasing dislocation density. The results clarify the difference between the grain size effect and the dislocation density effect on the stress hysteresis of nanocrystalline NiTi alloys.

1. Introduction

Superelasticity, which is closely related to the thermoelastic martensitic transformation, is known to be a significant functional property of near-equiatomic NiTi shape memory alloys (SMAs). The stress-induced transformation upon loading together with the reverse transformation between a body-centred cubic B2 phase and a monoclinic B19′ phase gives rise to a large reversible strain (~8%). Stress hysteresis is a typical characteristic of the superelastic NiTi alloys, which represents the stress difference of forward and inverse transformation during the superelastic loading and unloading process. The generation and motion of internal interfaces during forward and reverse transformation dissipate considerable mechanical energy, which results in a macroscopic stress hysteresis.

The development of microscale devices in recent years calls for NiTi alloys with small dimensions and high yield strengths. Reducing grain size down to the nanoscale can efficiently enhance the strengths of NiTi shape memory alloys (SMAs) [1–5]. In nanocrystalline NiTi alloys, the grain size affects the characteristics of both thermal-induced martensitic transformations and stress-induced transformations [6–12]. Previous experimental studies show that reducing the grain size can significantly reduce the stress hysteresis of polycrystalline NiTi alloys prepared by cold-rolling (42% thickness reduction) and annealing (at temperatures of 250–600 °C), especially when the grain size falls to the nanoscale (10–100 nm) [6–8]. The authors attributed the effect to the increase in phase interfacial energy (austenite/martensite interface) with a decrease in grain size, which is closely related to an incomplete phase transformation [6–8]. In their description, when the state of the system moves from one metastable local minimum (austenite) to the other (martensite), energy is dissipated, and the amount is equal to the free energy change [7,13]. The free energy change of the grains before and after martensitic nucleation decreases with increasing phase interfacial energy, which leads to a decrease in stress hysteresis [6–8]. However, in their studies, incomplete annealing processes (250–600 °C) were applied [6–8], and high-density dislocations could be encountered. The samples in those studies [6–8] contained the effect of both grain size and dislocation density. It was proposed that dislocation density affects the stress-induced martensitic transformation behaviour (i.e., stress hysteresis, critical transformation stress) of the NiTi alloys [14–16]. Therefore, the effect of grain sizes on stress hysteresis is

* Corresponding author.
E-mail address: lishancui63@126.com (L.S. Cui).

http://dx.doi.org/10.1016/j.jallcom.2016.07.168
0925-8388/

difficult to analyse in samples with different dislocation densities. Related to this, a molecular dynamics simulation of the nanoscale NiTi samples, studied by Zhang et al. [17], shows a similar size effect on the stress hysteresis, which is closely related to the difference in free energy states between interior and surface regions. However, in this study, the hysteresis is exactly affected by the sample size (1.5–20 nm in diameter), not grain size.

Reviewing this literature, it is unclear and meaningful whether this grain size effect is compatible with samples containing few dislocations that transform completely. The aim of the present work is to study the grain size effect on the stress hysteresis of martensitic transformation in nanocrystalline NiTi alloy, which is crystallized from amorphous phase and in which few dislocations could be encountered. In contrast to previous reports, our result shows that the stress hysteresis increases with decreasing grain size.

2. Experimental procedures

A near-equiatomic NiTi alloy wire with a nominal composition of Ni-49.5%at.Ti was acquired from the General Research Institute for Non-Ferrous Metals, China. The wire of 0.46 mm in diameter was annealed at 750 °C for 90 s under the protection of argon followed by air cooling and then cold drawn into diameters of 0.36 mm and 0.23 mm, effecting area reductions of approximately 75% and 39% (39% area reduction is close to a 42% thickness reduction upon cold-rolling in Ref. [7]), respectively. The samples having a length of 100 mm cut from the wire 0.23 mm in diameter were annealed in air at 400 °C, 450 °C and 500 °C for 0.6 ks, and the samples cut from the wire of 0.36 mm in diameter were annealed in air at 300 °C, 350 °C, 400 °C and 450 °C for 0.6 ks. The average grain size of the samples was measured by transmission electron microscopy (TEM). Samples used for TEM observation were mechanically polished and finally ion milled using a Gatan 691 PIPS. The TEM observation was carried out using a FEI Tecnai F20 (operating at 200 kV) equipped with a Gatan slow scan CCD camera. Small samples (approximately 10 mg) for differential scanning calorimeter (DSC) experiments (using a Netzsch DSC 204 F1 Phoenix) were cut from the wires. The cold-drawn samples were subjected to DSC experiments in the range of 40–450 °C and the annealed samples in the range of −100 to 120 °C with a heating/cooling rate of 10 °C/min. The tensile test was carried out using a WDT II-20 type tensile machine using a tensile speed of 3.0 mm/min at room temperature. The stress hysteresis was acquired by measuring the stress difference between the stresses of the 3% strain in the upper plateau and the 2.5% strain in the lower plateau as specified by the ASTM standard [18].

3. Results

3.1. Microstructure of the samples before annealing

Fig. 1 shows the TEM micrographs and DSC analysis of the samples before annealing. Fig. 1(a) shows a TEM bright-field image and a corresponding SAED pattern of the sample with 75% area reduction. The SAED pattern shows significant broad diffuse rings corresponding to the amorphous phase. It is seen that the sample contains nanograins embedded in an amorphous NiTi matrix. Fig. 1(b) shows the TEM analysis of the sample with 39% area reduction. The SAED pattern shows sharp polycrystalline diffraction

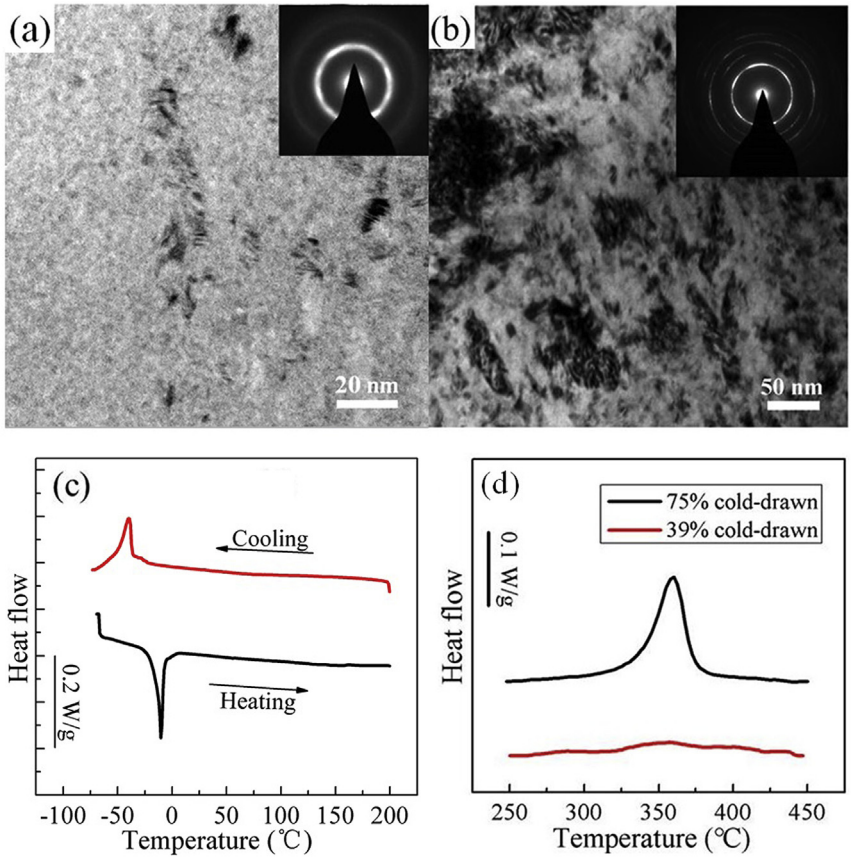

Fig. 1. The microstructure analysis of the samples before annealing. The TEM bright-field image and corresponding SAED pattern of (a) the 75% area reduced sample and (b) the 39% area reduced sample; (c–d) the DSC analysis of the samples before and after cold drawing, respectively.

rings, which indicate that there is no amorphous phase in the sample. The bright-field image reveals high-density dislocations in the sample. Fig. 1(c) shows the DSC analysis of the sample before cold drawing. It can be seen that the transformation temperatures M_s and M_f are approximately −27 °C and −55 °C, respectively. Fig. 1(d) shows the DSC analysis of cold-drawn samples. The DSC curve of the sample with 75% area reduction (black) reveals an exothermic peak in the range of 330–370 °C, which corresponds to the crystallization of amorphous phase. The DSC curve of the sample with 39% area reduction (red) reveals no exothermic peak.

3.2. Microstructure and stress hysteresis of the annealed samples

3.2.1. Sample with 75% area reduction

Fig. 2 shows the overall microstructure observations of the sample with 75% area reduction after annealing. Fig. 2(a) shows the bright-field TEM microstructures and corresponding SAED pattern of the sample annealed at 400 °C for 0.6 ks. The microstructure shows a completely nanocrystalline structure, and the SAED pattern reveals no diffused ring, which indicates that the amorphous phase has been fully crystallized after annealing. Fig. 2(b) shows the grain size distribution of the sample annealed at 400 °C. The majority (~97%) of grains are smaller than 40 nm, with an average grain size of approximately 20 nm based on the manual measurement of 200 grains. Fig. 2(c) and (d) show the bright-field TEM microstructures and corresponding SAED patterns of the samples annealed at 450 °C and 500 °C, respectively. The average grain sizes of these two samples are approximately 53 nm and 108 nm, respectively. An average grain size of approximately 257 nm of 550 °C annealed sample was also acquired by the same method. The high resolution TEM observations show that few dislocations could be found in the annealed samples. Fig. 2(e) shows the relationship between the average grain size and annealing temperature, and Fig. 2(f) reveals the DSC analysis of the samples after annealing. In Fig. 2(f), it can be seen that only the B2 ↔ R transformation was detected for the samples annealed at 400 °C and 450 °C. A two-stage B2 ↔ R ↔ B19′ transformation was detected for the samples annealed at 500 °C. The R → B19′ transformation temperature M_s is approximately −76 °C for the samples annealed at 500 °C, which is much lower than that for the sample before cold drawing (−27 °C). This grain size effect is consistent with the results reported recently [9–13].

Fig. 3(a) shows the tensile stress–strain curves of the annealed samples with 75% area reduction. All annealed samples exhibit flow stress upon loading and unloading, which demonstrated Lüders-type deformation behaviour during stress-induced martensitic transformation [19–22]. The sample annealed at 550 °C does not experience the reverse transformation because the stress for the inverse transformation is close to 0 MPa. Therefore, we cannot acquire the hysteresis information in the samples annealed at temperatures higher than 550 °C. The hysteresis of these samples corresponding to the grain size is shown in Fig. 3(b). Obviously, the stress hysteresis increases with decreasing grain size, which shows a reverse effect to the results reported recently [6–8].

3.2.2. Sample with 39% area reduction

Fig. 4 shows the microstructure analysis of the sample with 39% area reduction annealed at 300 °C, 400 °C and 450 °C. From the bright-field image of the sample annealed at 300 °C shown in Fig. 4(a), it is seen that many dislocations were encountered, and there is no recrystallized grain generated in the sample, which indicates that no recrystallization occurred during annealing. In the 400 °C annealed sample (as shown in Fig. 4(b)), most of the area recrystallizes to nanograins, and the dislocation density is less than the 300 °C annealed sample. In the 450 °C annealed sample (as shown in Fig. 4(c)), the recrystallized grains are larger, and the dislocation density is lower than that of the 400 °C annealed sample. Fig. 4(d) shows the dislocation density and grain size of the annealed samples measured by the Williamson–Hall method applying the XRD experiments. It is shown that the dislocation density decreases and the grain size increases with increasing annealing temperature.

Fig. 5 shows the hysteresis analysis of the samples with 39% area reduction after annealing. From the stress–strain curves of the samples in Fig. 5(a), it is seen that when annealing at higher temperatures (400 °C and 450 °C), the samples experience Lüders-type

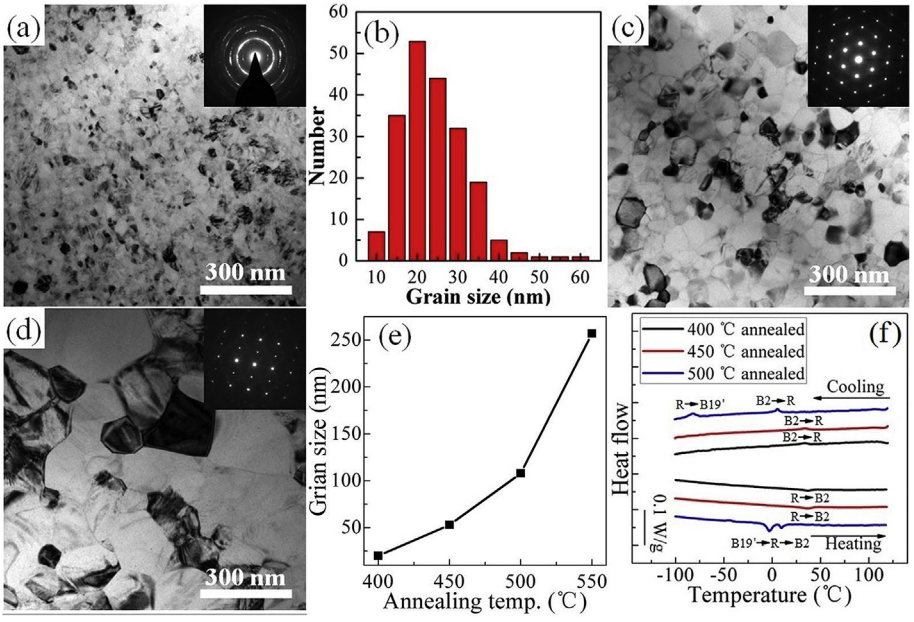

Fig. 2. The microstructure analysis of the annealed samples with 75% area reduction. (a) the TEM bright-field image and corresponding SAED pattern of the 400 °C annealed sample; (b) the grain size distribution of the 400 °C annealed sample; the TEM bright-field image and corresponding SAED pattern of the samples annealed at (c) 450 °C and (d) 500 °C; (e) the average grain size of the samples with different annealing temperatures; (f) DSC analysis of the samples after cold annealing.

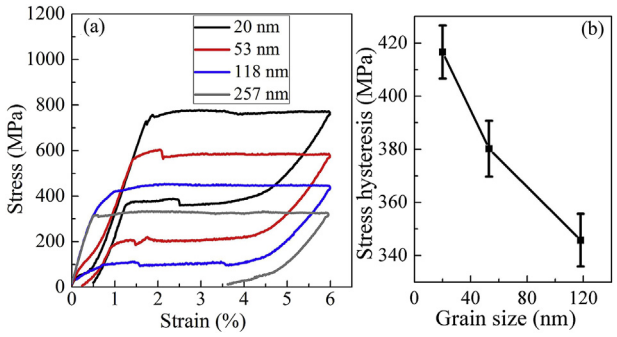

Fig. 3. The stress hysteresis analysis of the annealed samples with 75% area reduction. (a) The stress–strain curves; (b) the relationship between stress hysteresis and grain size.

deformation. With decreasing annealing temperature (350 °C), the deformation type tends to be homogeneous. When annealing at 300 °C, the samples experience absolutely homogeneous deformation. Fig. 5(b) shows the relationship between stress hysteresis and annealing temperature. It is seen that the stress hysteresis of these samples decreases with decreasing annealing temperature. From the results of the samples with 39% area reduction presented above, it can be seen that both tension stress–strain curves and the size effect on stress hysteresis are similar to the results acquired by A Ahadi et al. [7,8]. Because the grain size of the samples increases with increasing annealing temperature, we can deduce that the samples reveal an inverse grain size effect on stress hysteresis in contrast to the sample with 75% area reduction.

4. Discussion

4.1. Activation energy for grain boundary migration

Fig. 2(b) shows a non-bimodal grain size distribution, which indicates that no secondary grain growth occurs [23]. The results in Fig. 2(e) show that the average grain diameter increases with increasing annealing temperature. It was proposed that when grain growth occurs, the variation with time t of the grain size d can be given by Refs. [24,25]:

$$d^2 = d_0^2 + Kt \tag{1}$$

where d_0 is the initial grain size, and K is the grain boundary migration rate, which exhibits the Arrhenius behaviour [24–28]:

$$K = K_0 \exp\left(-\frac{Q_m}{2.3RT}\right) \tag{2}$$

where K_0 and R are constant, Q_m is the activation energy for the grain boundary migration, and T is the temperature. According to Eqs. (1) and (2), the grain size d can be described by

$$d^2 = d_0^2 + K_0 t \exp\left(-\frac{Q_m}{2.3RT}\right) \tag{3}$$

As the results show in Fig. 1, most of the area of the sample with 75% area reduction was vitrified after cold drawing. Because the annealed samples were mostly crystallized from the amorphous phase, we can suppose that $d_0 = 0$. Eq. (3) can be expressed as

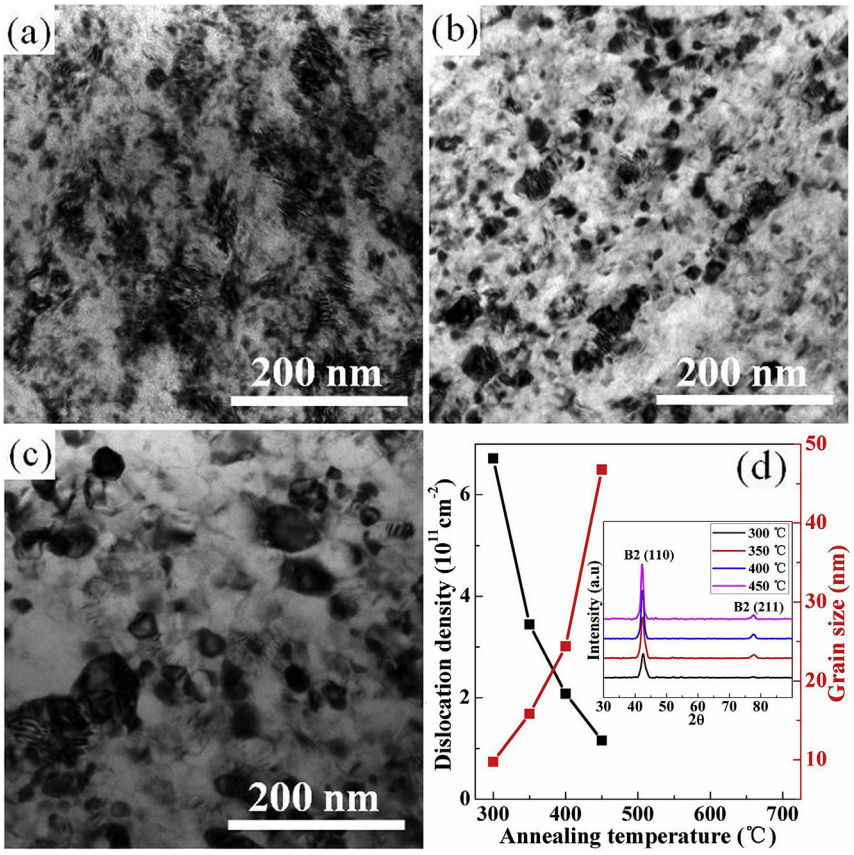

Fig. 4. The microstructure analysis of the annealed samples with 39% area reduction. (a–c) The TEM bright-field image and corresponding SAED pattern of the samples annealed at 300 °C, (b) 400 °C and (c) 450 °C, respectively; (d) the dislocation density and grain size of the samples with different annealing temperatures.

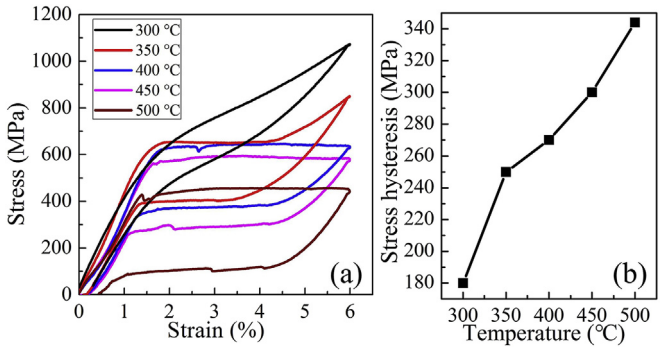

Fig. 5. The stress hysteresis analysis of the annealed samples with 39% area reduction. (a) The stress–strain curves; (b) the relationship between stress hysteresis and annealing temperature.

$$\ln(d) = -\frac{Q_m}{4.6RT} + \frac{1}{2}\ln(K_0 t) \quad (4)$$

Fig. 6 is the Arrhenius plot of d of the sample with 75% area reduction; the red symbols are the experimental results, the black line is the linear fitting result of the red symbols, and the slope is $(-9.2 \pm 0.4) \times 10^3$ K. We can extract the activation energy for grain boundary migration Q_m = 353.6 ± 15.3 kJ/mol (approximately 3.55 ± 0.15 eV), which is consistent with the activation energy of NiTi alloy reported previously (approximately 3.12 ± 0.05 eV) [28].

4.2. Microstructure difference of the annealed samples

The results of Figs. 3 and 5 show absolutely opposite grain size effects on the stress hysteresis between the samples with 75% and 39% area reduction. From the TEM observation of the annealed samples, it is seen that the microstructures of these samples are different. Very few dislocations could be found in the former sample, which indicate an intrinsic grain size effect on stress hysteresis. However, there are many dislocations in the latter sample. The reason for this difference is the microstructural difference of the initial samples before annealing. The results of Fig. 1 show that a larger cold-drawn strain (75% area reduction) induces amorphous phase in most of the areas of the sample, and the amorphous phase crystallized at a range of 330–370 °C. Therefore, the annealed samples experience a crystallization process, which ensures that the samples reveal few dislocations. A lower cold-drawn strain (39% area reduction) cannot induce amorphous phase (as shown in Fig. 1(b)). The 300 °C annealed samples experience a recovery process, and the 400 °C and 450 °C annealed samples experience a partial recrystallization process. These annealed samples contain many dislocations, and the density decreases with increasing annealing temperature, as the results show in Fig. 4(d). Therefore, we can deduce that the hysteresis of the samples with 39% area reduction exactly decreases with increasing dislocation density but not grain size.

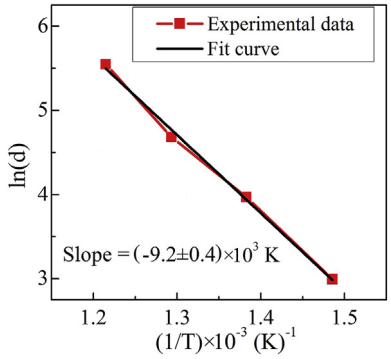

Fig. 6. Arrhenius plot of the mean grain diameter of the sample with 75% area reduction, the red symbols are the experimental results, and the black line is the linear fitting result of the red symbols. (For interpretation of the references to colour in this figure legend, the reader is referred to the web version of this article.)

4.3. Dislocation effect on stress hysteresis

Delville et al. reported an effect of dislocations on stress-induced martensitic transformation [14]. Their results show that the accumulation of dislocations affects the shape of the superelastic stress–strain curve [14]. We propose that in the samples with 39% area reduction, the martensitic phase nucleates at the stress concentration areas induced by the dislocations. The nucleation sites increase with increasing dislocation density, which increases the interface between the martensite and parent phases during nucleation and therefore increases the interfacial energy. The effect of phase interfaces on stress hysteresis of nanocrystalline NiTi alloy was analysed by Aslan et al. [7,8]. Their results support that the stress hysteresis decreases with increasing interfacial energy [7,8]. Therefore, in the samples with 39% area reduction, the increasing dislocation density reduces the hysteresis of the stress-induced martensitic transformation.

4.4. Grain size effect on stress hysteresis

The grain size effect on hysteresis as illustrated in Fig. 2 shows that the stress hysteresis of nanocrystalline NiTi alloy increases with decreasing grain size. It is known that the grain boundary plays an important role in nanocrystalline materials [19–22,29–33]. Nanostructures are usually considered as composites consisting of crystalline grain cores and an amorphous grain boundary "phase" [21,34]. Fig. 7 presents the schematic representation of the deformation process of nanocrystalline NiTi alloy during superelastic cycling. Fig. 7(a) presents a schematic image of the grain core and boundary distribution; the dark grey regions represent grain cores, and the light grey regions represent grain boundaries. Fig. 7(b) presents the schematic image of stress–strain curves of the grain cores and boundaries during superelastic cycling. During loading, the grain cores experience a transformation process (AB) and reveal a transformation strain. To accommodate the transformation strain of the grain cores, grain boundaries experience a plastic tensile deformation (A′B′). During unloading, the grain cores experience an inverse transformation process (BCD) and return to the original length. The grain boundaries elastically unload to point C′ first. The boundaries are then compressed by the inverse-transforming grain cores, and plastic deformation (D′E′) occurs.

The plastic deformation of grain boundaries and the generation and motion of internal interfaces of grain cores contribute to the energy dissipation during superelastic cycling. The energy dissipation per volume of grain cores (E_c) and boundaries (E_b) is presented as dark grey areas and light grey areas in Fig. 7(b), respectively. E_b^1 and E_b^2 are the energy dissipation of boundaries during loading and unloading, respectively; therefore, $E_b = E_b^1 + E_b^2$. It is known that the yield strength of the grain boundary is higher than that of the grain core when the grain size is larger than the critical size (approximately 10 nm), which indicates that the Hall–Petch relationship is reasonable [20,21,31,32]. Because the flow stress of stress-induced transformation is less than the stress for that of plastic deformation, we can deduce that the yield strength of the grain boundary (A′) is higher than the flow stress of

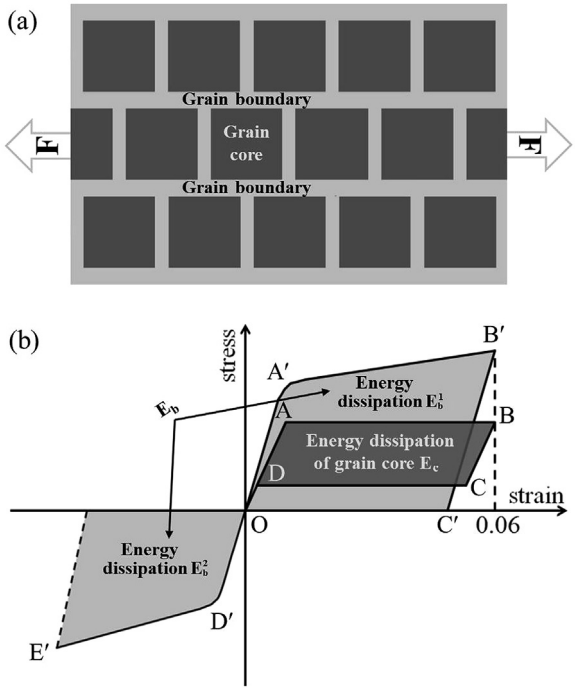

Fig. 7. Schematic representation of the deformation process of nanocrystalline NiTi alloy during superelastic cycling. (a) The schematic image of the grain core and boundary distribution; the dark grey regions represent grain cores, and the light grey regions represent grain boundaries; (b) the schematic image of stress–strain curves and energy dissipation of the grain cores and boundaries during the superelastic cycling; the dark grey area represents the energy dissipation of the grain cores E_c, and the dark grey areas represent the energy dissipation of the grain boundaries E_b. E_b^1 and E_b^2 are the energy dissipations of the grain boundaries during loading and unloading, respectively, and $E_b = E_b^1 + E_b^2$.

the grain core (A). Therefore, it can be seen in Fig. 7(b) that $E_b^1 > E_c$.

The energy dissipation per volume of the sample is

$$E = \phi_c E_c + \phi_b E_b = E_c + \phi_b (E_b - E_c) \quad (5)$$

where ϕ_c and ϕ_b are volume fractions of grain cores and boundaries, respectively. It is known that, in nanocrystalline metals, ϕ_b increases with decreasing grain size [20,21,31,32]. Because $E_b = E_b^1 + E_b^2 > E_c$, we can deduce from Eq. (5) that the energy dissipation of the whole sample increases with decreasing grain size, which result in increased stress hysteresis.

5. Summary and conclusions

The grain size effect on the stress hysteresis of nanocrystalline NiTi alloy during superelastic cycling was investigated by testing two types of samples with 75% and 39% area reduction. From the results obtained in this study, the following interesting conclusions were obtained:

1. The activation energy for grain boundary migration of the NiTi alloy was analysed and found to be 353.6 ± 15.3 kJ/mol.
2. The results of the annealed samples with 39% area reduction suggest that the dislocation density affects the stress hysteresis of nanocrystalline NiTi alloy. The increase in phase interfacial energy reduces the energy dispassion, which reduces the stress hysteresis of nanocrystalline NiTi alloy during the superelastic cycling.
3. The results of the annealed samples with 75% area reduction suggest that the stress hysteresis increases with decreasing grain size in nanocrystalline NiTi alloy. The plastic deformation of grain boundaries affects the stress hysteresis of nanocrystalline NiTi alloy. The volume fraction of grain boundaries increases, and the boundary strength decreases with decreasing grain size, which increases the stress hysteresis during the superelastic cycling.

Acknowledgements

This work was supported by the key program project of the National Natural Science Foundation of China (51231008), the National 973 programs of China (2012CB619403) and the Key Project of Chinese Ministry of Education (313055).

References

[1] V.G. Pushin, V.V. Stolyarov, R.Z. Valiev, T.C. Lowe, Y.T. Zhu, Nanostructured TiNi-based shape memory alloys processed by severe plastic deformation, Mater. Sci. Eng. A 410–411 (2005) 386–389.
[2] A.V. Sergueeva, C. Song, R.Z. Valiev, A.K. Mukherjee, Structure and properties of amorphous and nanocrystalline NiTi prepared by severe plastic deformation and annealing, Mater. Sci. Eng. A 339 (2003) 159–165.
[3] J. Ye, R.K. Mishra, A.R. Pelton, A.M. Minor, Direct observation of the NiTi martensitic phase transformation in nanoscale volumes, Acta Mater. 58 (2010) 490–498.
[4] E. Prokofiev, D. Gunderov, A. Lukyanov, V. Pushin, R. Valiev, Mechanical behavior and stress-induced martensitic transformation in nanocrystalline $Ti_{49.4}Ni_{50.6}$ alloy, Mater. Sci. Forum 584–586 (2008) 470–474.
[5] R. Valiev, D. Gunderov, E. Prokofiev, V. Pushin, Y.T. Zhu, Nanostructuring of TiNi alloy by SPD processing for advanced properties, Mater. Trans. 49 (2008) 97–101.
[6] Q.P. Sun, Y.J. He, A multiscale continuum model of the grain-size dependence of the stress hysteresis in shape memory alloy polycrystals, Int. J. Solids Struct. 45 (2008) 3868–3896.
[7] A. Ahadi, Q.P. Sun, Stress hysteresis and temperature dependence of phase transition stress in nanostructured NiTi-Effects of grain size, Appl. Phys. Lett. 103 (2013) 021902.
[8] A. Ahadi, Q.P. Sun, Stress-induced nanoscale phase transition in superelastic NiTi by in situ X-ray diffraction, Acta Mater. 90 (2015) 272–281.
[9] T. Waitz, T. Antretter, F. Fischer, N. Simha, H. Karnthaler, Size effects on the martensitic phase transformation of NiTi nanograins, J. Mech. Phys. Solids 55 (2007) 419–444.
[10] T. Waitz, V. Kazykhanov, H. Karnthaler, Martensitic phase transformations in nanocrystalline NiTi studied by TEM, Acta Mater. 52 (2004) 137–147.
[11] T. Waitz, H. Karnthaler, Martensitic transformation of NiTi nanocrystals embedded in an amorphous matrix, Acta Mater. 52 (2004) 5461–5469.
[12] T. Waitz, W. Pranger, T. Antretter, F. Fischer, H. Karnthaler, Competing accommodation mechanisms of the martensite in nanocrystalline NiTi shape memory alloys, Mater. Sci. Eng. A 481–482 (2008) 479–483.
[13] R. Ahluwalia, S. Quek, D.T. Wu, Simulation of grain size effects in nanocrystalline shape memory alloys, J. Appl. Phys. 117 (2015) 244305.
[14] R. Delville, B. Malard, J. Pilch, P. Sittner, D. Schryvers, Transmission electron microscopy investigation of dislocation slip during superelastic cycling of Ni-Ti wires, Int. J. Plasticity 27 (2011) 282–297.
[15] C.P. Frick, A.M. Ortega, J. Tyber, A.El.M. Maksound, H.J. Maier, Y. Liu, K. Gall, Thermal processing of polycrystalline NiTi shape memory alloys, Mater. Sci. Eng. A 405 (2005) 34–49.
[16] Y. Liu, Z. Xie, J. Van Humbeeck, L. Delaey, Asymmetry of stress–strain curves under tension and compression for NiTi shape memory alloys, Acta mater. 46 (1998) 4325–4338.
[17] Z. Zhang, X. Ding, J. Sun, T. Suzuki, T. Lookman, K. Otsuka, X. Ren, Non-hysteretic superelasticity of shape memory alloys at the nanoscale, Phys. Rev. Lett. 111 (2013) 145701.
[18] Standard Test Method for Tension Testing of Nickel-titanium Superelastic Materials, ASTM Stand, 2015. F2516-14.
[19] M. Peterlechner, T. Waitz, C. Gammer, T. Antretter, Martensitic phase transformations of nanocrystalline NiTi shape memory alloys processed by repeated cold rolling, Int. J. Mater. Res. 102 (2011) 634–642.
[20] S. Yip, Nanocrystals: the strongest size, Nature 391 (1998) 532–533.
[21] H. Li, H. Choo, Y. Ren, T.A. Saleh, U. Lienert, P.K. Liaw, F. Ebrahimi, Strain-dependent deformation behavior in nanocrystalline metals, Phys. Rev. Lett. 101 (2008) 015502.
[22] J. Schiøtz, F.D. Di Tolla, K.W. Jacobsen, Softening of nanocrystalline metals at very small grain sizes, Nature 391 (1998) 561–563.
[23] T. Bormann, B. Müller, M. Schinhammer, A. Kessler, P. Thalmann, M. de Wild, Microstructure of selective laser melted nickel–titanium, Mater. Charact. 94 (2014) 189–202.
[24] M. Montagnat, P. Duval, Rate controlling processes in the creep of polar ice, influence of grain boundary migration associated with recrystallization, Earth Planet. Sci. Lett. 183 (2000) 179–186.

[25] A.J. Gow, On the rate of growth of grains and crystals in south polar firn, J. Glaciol. 8 (1969) 241–252.
[26] B. Müller, Natural formation of nanostructures: from fundamentals in metal heteroepitaxy to applications in optics and biomaterials science, Surf. Rev. Lett. 8 (1 & 2) (2001) 169–228.
[27] J.G. Amar, F. Family, Critical cluster size: island morphology and size distribution in submonolayer epitaxial growth, Phys. Rev. Lett. 74 (1995) 2066–2069.
[28] X. Wang, J.J. Vlassak, Crystallization kinetics of amorphous NiTi shape memory alloy thin films, Scr. Mater. 54 (2006) 925–930.
[29] J. Schiøtz, K.W. Jacobsen, A maximum in the strength of nanocrystalline copper, Science 301 (2003) 1357–1359.
[30] K. Maung, J.C. Earthman, F.A. Mohamed, Inverse Hall–Petch behavior in diamantane stabilized bulk nanocrystalline aluminum, Acta Mater. 60 (2012) 5850–5857.
[31] Y. Tang, E.M. Bringa, M.A. Meyers, Inverse Hall–Petch relationship in nanocrystalline tantalum, Mater. Sci. Eng. A 580 (2013) 414–426.
[32] M. Dao, L. Lu, R.J. Asaro, J.T.M. De Hosson, E. Ma, Toward a quantitative understanding of mechanical behavior of nanocrystalline metals, Acta Mater. 55 (2007) 4041–4065.
[33] J.R. Trelewicz, C.A. Schuh, The Hall–Petch breakdown in nanocrystalline metals: a crossover to glass-like deformation, Acta Mater. 55 (2007) 5948–5958.
[34] H.S. Kim, A composite model for mechanical properties of nanocrystalline materials,, Scr. Mater. 39 (1998) 1057–1061.